q-Gaussian Tsallis line shapes for Raman spectroscopy: Fitting simulations and data analysis

Amelia Carolina Sparavigna

Department of Applied Science and Technology, Polytechnic University of Turin, Italy

Email: amelia.sparavigna@polito.it

Abstract

q-Gaussians are probability distributions having their origin in the framework of Tsallis statistics. A continuous real parameter q is characterizing them so that, in the range $1 < q < 3$, the q-functions pass from the usual Gaussian form, for q close to 1, to that of a heavy tailed distribution, at q close to 3. The value q=2 corresponds to the Cauchy-Lorentzian distribution. This behavior of q-Gaussian functions can be used for the analysis of Raman spectra, where Lorentzian and Gaussian profiles are among the line shapes most used to fit the spectral bands. In the first part of this discussion, we consider fitting simulations with q-Gaussian Tsallis lines and comparison to analyses made by means of Lorentzian and Gaussian lines. In the second part we show several examples of fitting experimental data.

Keywords: q-Gaussian distribution, Gaussian distribution, Cauchy distribution, Lorentzian distribution, Voigt distribution, Pseudo-Voigt function, Carbonaceous Materials, Biochar, Synthetic Organic Pigments, Raman spectroscopy, EPR spectroscopy, Tsallis line shape, IR spectroscopy.

Zenodo, April 27, 2023. DOI: 10.5281/zenodo.7856363

1. Introduction

The q-Gaussian functions are probability distributions proper of the Tsallis statistics (Tsallis, 1988, Hanel et al., 2009). These functions are based on a generalized form of the exponential function (see for instance the discussion in Sparavigna, 2022), where a continuous real parameter q is characterizing it. When q is going to 1, the q-exponential becomes the usual exponential function. The q-Gaussian is therefore the Tsallis generalization of the Gaussian distribution. In the range of q-parameter from 1 to 3, we pass from the Gaussian to a heavy tailed distribution. The value q=2, (Naudts, 2009), corresponds to the Cauchy distribution, also known in physics as the Lorentzian distribution; then, the q-Gaussian function is the generalization of the Lorentzian distribution too. In heavy tail regions, the function is equivalent to the Student's distribution. The change of q-parameter is therefore allowing the q-Gaussian to pass from Gaussian function to Lorentzian distribution.

The q-Gaussian had been proposed in 2003 by Howarth et al. as a line shape suitable for describing electron paramagnetic resonance (EPR) spectra, "and possibly nuclear magnetic resonance (NMR) spectra as well". In the article by Howarth et al., the q-Gaussian function is not mentioned in this manner, but as the "Tsallis lineshape". Howarth and coworkers stressed that the Tsallis line shape is generalizing the Gaussian and Lorentzian functions "widely used in simulations". The researchers compared the proposed Tsallis line shape with experimental EPR spectra, evidencing that the q-line shape "often provides a better approximation of the experimental spectrum". Yu. A. Koksharov, 2015, for the electron magnetic resonance study of nanoparticles, proposed to use the decomposition of the spectra with the Tsallis distributions (that is the q-Gaussian functions). The method has been tested on a two-component spectrum of colloidal magnetite nanoparticles and on broad spectra of iron-containing

nanoparticles. In an article of 2009, by Yuanlu Li, the "Tsallis distribution" is given as a function which is facilitating the generalization of Gaussian and Lorentzian line shapes by varying the parameter q "as a model of the individual band to correctly assign overlapping bands". Yuanlu Li simulated the bands by computer and analyzed the experimental infrared spectrum of 1,2-bromofluoroethane.

The Raman bands are usually given as characterized by Lorentzian or Gaussian distributions, or by a *linear combination* (pseudo-Voigt distribution) or by the *convolution* of them (Voigt distribution) (Meier, 2005). In a previous discussion (Sparavigna, 2023a, 2023b), we have proposed the q-Gaussians for Raman spectroscopy showing that they are properly mimicking pseudo-Voigt, Voigt functions and the Egelstaff-Schofield spectral line shapes. We have also discussed the Raman spectroscopy, for what is regarding the D and G bands of carbon-based materials[1]. Here we consider a series of simulations to understand how the fitting by means of q-Gaussians is different from that obtained with Gaussian and Lorentzian lines. Then, we apply q-Gaussians to the fitting of several experimental data.

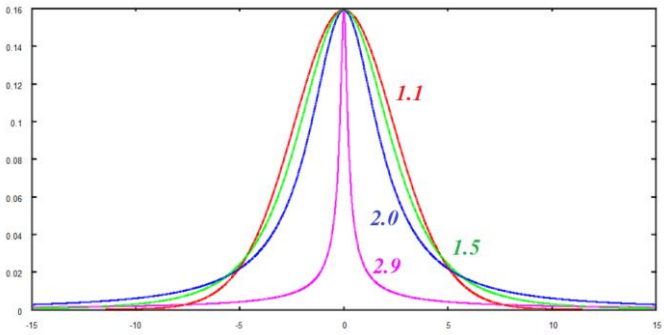

Fig. 1: q-Gaussian functions, for different q indices, from 1.1 (quasi-Gaussian) to 2.9 (over-Lorentzian). The blue curve is the Lorentzian line shape.

2. The q-Gaussians

As given by Umarov et al., 2008, the q-Gaussian function is:

$$f(x) = Ce_q(-\beta x^2) \quad (1),$$

where $e_q(.)$ is the q-exponential function and C a scale constant. In the exponent, we use $\beta = 1/(2\sigma^2)$. The q-exponential has the expression:

$$exp_q(u) = [1 + (1-q)u]^{1/(1-q)} \quad (2)\,.$$

The plots in the Figures 1 and 2a are showing the behaviour of this exponential for different q values. Note that, for q less than one, the function is different from zero on a limited interval.

1 The G-band is the main Raman mode in graphite and graphene, linked to the planar configuration sp^2 bonded carbon, which is constituting the graphene layers (Application Note). "The band position is pretty much independent of excitation laser frequency" (Application Note). The D-band is the "disorder band" or the "defect band". "This band is linked to the ring breathing mode from sp^2 carbon rings … The band is typically very weak in graphite and is typically weak in graphene as well. If the D-band is significant, it indicates that there are a lot of defects in the material" (Application Note).

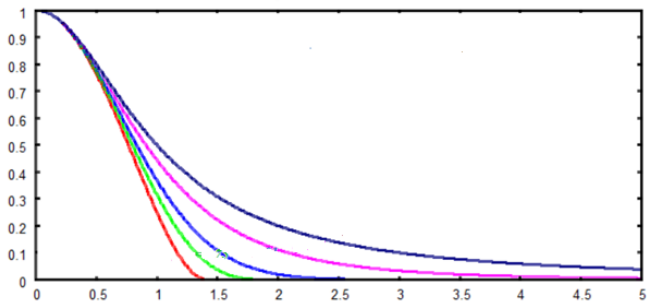

Fig.2a: q- exponential functions, where the blue curve is representing a Lorentzian function (q=2). The pink curve corresponds to q=1.5 and light blue to q= 1.01, practically a Gaussian function. The green curve is the q-Gaussian for q=0.75 and red curve for q=0.5. For $q < 1$, the function is different from zero in a limited interval. Being the line symmetric, only the right part of it is given in the figure.

The Half Width at Half Maximum of q line shape is given by: $\sqrt{2}\,\sigma\,\sqrt{(1-(1/2)^{1-q})/(1-q)}$.

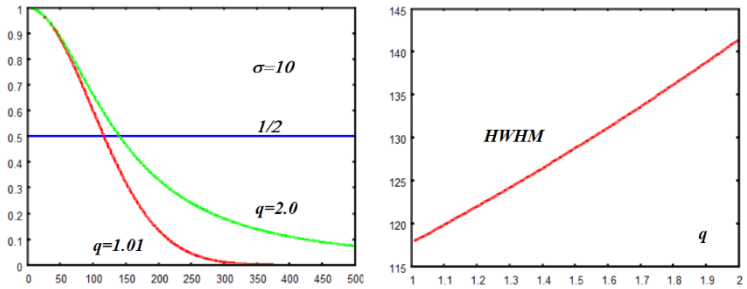

Fig.2b: q- exponential functions for q=1.01 and q=2 on the left, on the right the Half Width at Half Maximum as a function of q.

3. GLS, GLP, Voigt and synthetic lines

In Jain et al., 2018, comparisons are given among Gaussian-Lorentzian sum (GLS or Pseudo-Voigt) functions, Gaussian-Lorentzian product (GLP) functions, and Voigt functions. The framework is the peak fitting of X-ray photoelectron spectroscopy (XPS). "Plots of the GLS show that it is a better mathematical representation of a function that *is intermediate* between a pure Gaussian and a pure Lorentzian". The GLS also represents a better approximation of the Voigt function. A reason is in the fact that the "Voigt function looks like Gaussian for small x (i.e., near line center), and like Lorentzian for large x (i.e., out in line wings)" (Townsend, 2008), depending on the choice of parameters.

$$V(x;\sigma,\gamma) \equiv \int_{-\infty}^{\infty} G(x';\sigma)L(x-x';\gamma)\,dx',$$

$$G(x;\sigma) \equiv \frac{e^{-x^2/(2\sigma^2)}}{\sigma\sqrt{2\pi}}, \quad L(x;\gamma) \equiv \frac{\gamma}{\pi(x^2+\gamma^2)}.$$

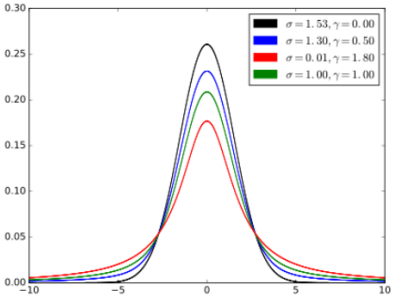

Fig.3: Definition of the Voigt convolution and related functions (plot courtesy Shiyu Ji, under CC BY-SA 4.0 license, https://en.wikipedia.org/wiki/Voigt_profile#/media/File:VoigtPDF.svg .

Regarding the GLP functions, “because of the more compact nature of the Gaussian, the GLP does not have significant wings" (Jain et al., 2018). GLS, that are also known as Pseudo-Voigt functions, have wings with different consistency, and the same is also true for the q-Gaussians, depending on the value of parameter q.

Jain et al. considered XPS. “In the theory of X-ray photoelectron spectroscopy, natural line shapes are generally assumed to be Lorentzian. There are, however, reasons why this line shape may not be observed experimentally” (Jain et al., 2018). After specific discussions, Jain and coworkers explain it is possible to argue that “when a set of photoelectrons, which may inherently have a Lorentzian line shape, is perturbed by a spectrometer and/or the broadening mechanisms mentioned above, one would expect the final signal to have at least some Gaussian character”. Then, “it is plausible that many of the components of XPS narrow scans will be best defined and fit by peaks that have both Gaussian and Lorentzian character”. According to the researchers, “mathematically, the ‘purest’ way to handle this problem is to use a Voigt function”, (Jain et al., 2018), but GLS, GLP and other functions are generally proposed by several fitting packages. The same is true for the Raman spectroscopy: the purest line shape is considered being the Voigt one (Meier, 2005), but pseudo-Voigt and other functions are used too.

As stressed by Jain et al., there is “an *active area of research* [aiming] to determine which *synthetic function* is most appropriate in different situations”. “*However, … the most important test of a synthetic line shape is not the theory behind it but rather its effectiveness in fitting real data*”. For the Raman spectroscopy too, we can propose the investigation of new “synthetic” lines, and the q-Gaussian Tsallis function is one of them. Synthetic or real?

4. Physical reasons

Physical reasons for the q-Gaussians are based on Tsallis statistics, regarding fractal and granular matter. “The macroscopic stability of powder mixtures and other forms of granular or fibre matter might be associated with fractal sets … Under these circumstances, there is no reason for having a relevant "thermodynamic" energy proportional to a standard power of the mass of the system. Consequently, nonextensive phenomena could be present” (Tsallis, 1995).

The Tsallis statistics, with the use of q-parameter to evaluate the degree of nonextensivity of the system, has been proposed for the Stimulated Raman Scattering (SRS) in a collisionless plasma by Sharifi & Parvazian (2015). SRS involves a resonant decay of laser electromagnetic waves into scattered electromagnetic waves and electron plasma waves (EPW). “Most of the studies for SRS are derived in the frame of a fluid description, a Maxwellian distribution function, or a relativistic Maxwellian distribution function. However, many space and laboratory plasmas show a non-Maxwellian behavior” (Sharifi & Parvazian, 2015). According to Sharifi and Parvazian, new statistical approaches based on the generalization of Boltzmann–Gibbs entropy, have been proposed, according to the works by Alfred Rényi (1955) and Constantino Tsallis (1988). The statistics that Sharifi and Parvazian are using is the q-Gaussian, q-nonextensive velocity distribution, which is generalizing the Maxwellian distribution.

Regarding the profile of Raman scattering and fluorescence, the collisional broadening and the Doppler broadening are relevant (Demtröder, 1985). The Doppler shift is usually given with the Maxwellian distribution (Nienhuis & Schuller, 1977). Then, a q-nonextensive generalization is possible in the case of Raman scattering too (for neutron scattering, see please De Abreu et al., 2022, Guedes et al., 2019). For the Doppler effect on light scattering, let me stress the discussion proposed by Chandrasekhara Venkata Raman, in his letter of 1931.

5. Separating the overlapping peak signals

Besides the choice of the synthetic line shape, for fitting the experimental data it is required to establish the number and positions of the bands composing the Raman spectrum. This is fundamental for the problem of "separating overlapped peak signals (OPS)". Li et al., 2010, proposed it in the framework of Tsallis model and fractional-order differentiation. OPS "is a predominant aspect of signals processing of modern times. The separation of received signal and restoration of the desired ones have long been a problem in overlapped signals decomposition" (Li et al., 2010). Actually, OPS pertains to a wide range of applications, such as in communications, thermal analysis, nuclear-magnetic resonance, in spectroscopy in general, and in the X-ray diffraction, as told by Li and coworkers.

Here in the following, for starting the fitting simulations we consider OPS in the case of a composition of three spectral bands. The aim is that of simulating the fitting with the three bands D1, D3 and G, relevant for carbon-based materials. In fact, in Sparavigna, 2023a, the q-Gaussians had been proposed for the analysis of biochar, a carbonaceous material, considering data collected by Tagliaferro et al., 2020.

In Tagliaferro et al., 2020, in the Figure 6 of their paper we can find the Raman spectra for different biochar samples. Biochar is the solid residue of pyrolysis of biomass obtained by thermochemical decomposition at moderate temperatures under oxygen-limiting conditions (Bartoli & Giorcelli, 2022, Brassard et al., 2019, Han & Kim, 2008, Ok et al., 2015, 2018, Giorcelli et al., 2021, Das et al., 2021, Yasim-Anuar et al., 2022). The spectrum analysis made by Tagliaferro and coworkers is based on a synthetic line shape the authors proposed with the name "GauLor". It is a function producing a line shape with a "central" part which is Lorentzian and the "wings" that are Gaussian functions. According to the definition given by W. Demtröder, 1985, the central part of the line (kernel) is within the range determined by the Full Width at Half Maximum of the line, the wings are outside of it; in the GauLor line shape the onset of the Gaussian wings is given by a frequency threshold value determined by the best fit of all the Raman spectrum. Supposing the existence of a threshold within the Raman scan range, the GauLor has the onset of the Gaussian tail which can be very close to the center of the line or quite far from it.

One of the panels of the Figure 6 is based on a four-band model with bands G, D1, D3, D4 (we use the notation given by Sousa et al., 2020). To fit Tagliaferro et al. data by means of q-Gaussians, parameters q, β, C have been used for the q-Gaussian functions corresponding to the four bands. The parameters have been determined by minimizing the sum of the squares of deviations $\Delta^2 = \sum\left(f_{Data} - f_{q-Gau}\right)^2$ (the sum is made on sample points). The resulting fit is here shown in the Figure 4 (Sparavigna, 2023a).

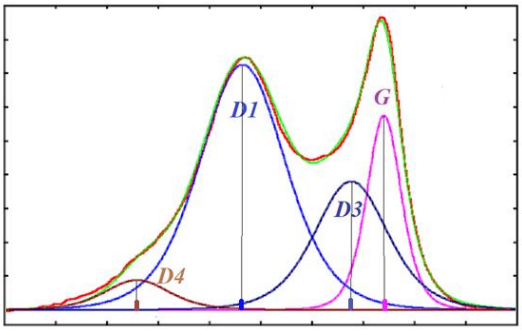

Fig. 4: The plot here given is obtained by means of four q-Gaussians, fitting data from Tagliaferro et al., 2020, regarding a biochar sample. Green (fit) and red (data) curves are in good agreement. The positions of the centers of the bands are also marked.

6. Fitting simulations

Looking at the Figure 4, it seems that Gaussian and Lorentzian functions could be suitable for fitting data as well as the q-Gaussians, but it is not so. Then, let us simulate some fitting cases to have specific

information about the role of the line shape. For simulations, let us consider just three peaks, D1, D3 and G. The synthetic curve to be fitted is given in the Figure 5. The position of the peaks is maintained fixed as in the Figure 4.

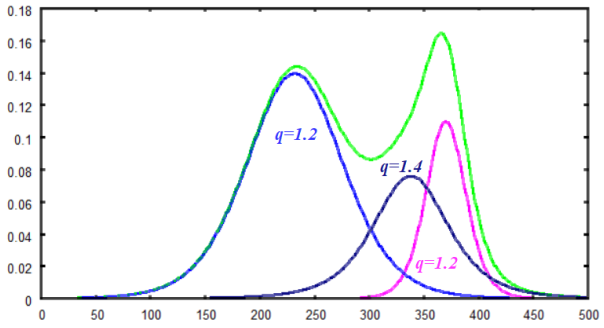

Fig. 5: The green curve here given is the curve that we will use for the first fitting simulations. It is given by the three q-Gaussians corresponding to D1, D3 and G, of the Fig. 4.

Therefore, we use three q-Gaussians with parameter q as in the Figure 5. Other parameters of the three q-Gaussians are: C=0.13956, σ=42.500 (D1), C=0.10971, σ=17.5 (G) and C=0.07600, σ=32.0 (D3). The curve provided by the sum of these three q-Gaussians (Fig.5) is our synthetic "experimental" data. This curve - from now on depicted in red - is given as a function of integers *n* (500 samples, that is *n* from 0 to 500, x-axis). A convenient scale is given for y-axis.

The fit of this red curve will be given in green color. The fitting calculation is obtained by minimizing the sum of the squares of the deviations $\Delta^2 = \sum(f_{red} - f_{green})^2$ iteratively (gradient method). The first best fit is proposed in the Figure 6. In this case, the values of parameter q for the tested q-Gaussians are constrained to the discretized values 1.01, 1.2, 1.4, 1.6, 1.8, and 2.0. q=1.01 is representing the Gaussian-like q-function. The positions of the centers of these q-Gaussians are fixed as that of Figure 5. The components of the fit are given by the blue and pink lines. Of course, the constrained q-Gaussian fit is providing a perfect fitting curve.

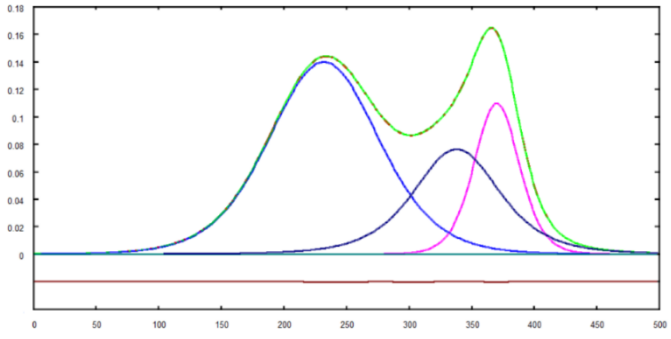

Fig. 6: Red curve is the curve to fit (the same as the green curve in Figure 5), and the green curve is the best fit (constrained q parameters). Curves are indistinguishable. The components are given by blue and pink lines. Fitting parameters are: q=1.2, C=0.13966, σ=42.416 (D1), q=1.2, C=0.10966, σ=17.416 (G) and q=1.4, C=0.0763, σ= 32.083 (D3). The sum of the squares of the deviations is $\Delta^2 = 4.1 \times 10^{-6}$ *. In the lower part of the image, the brown line is giving the difference between the red and the green line (the range is from -0.02 to 0.02). No appreciable difference is displayed.*

If we relax constraints about the values of the q-parameters, that is all values ranging from 1.01 to 2.0 are possible for the three bands, the best fit we obtain is given in the following Figure 7.

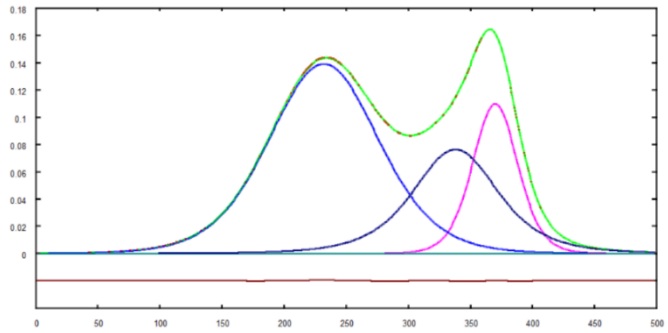

Fig. 7: Red curve is the curve to fit, and the green curve is the best fit (unconstrained q). Fitting parameters are: q=1.1875, C=0.13900, σ=42.750 (D1), q=1.1875, C=0.1096, σ=17.583 (G) and q=1.4125, C=0.07633, σ= 31.916 (D3). The sum of the squares of the deviations is $\Delta^2 = 1.0 \times 10^{-5}$ *. As in the previous figure, the brown line represents the difference between red and green line.*

Comparing the results given in the Figures 6 and 7, we could conclude that an uncertainty of ±0.01 is given about the value of fitting parameter q.

Let us change the curve to be used for simulations. Again, let us use three peaks, D1, D3 and G, as given in the Figure 8. The q-Gaussians parameters q are 1.2 (D1), 1.8 (G) and 1.4 (D3). Other parameters of the three q-Gaussians are: C=0.13956, σ=42.500 (D1), C=0.10971, σ=17.5 (G) and C=0.07600, σ=32.0 (D3). These parameters are the same of those for the simulation regarding the Figure 5.

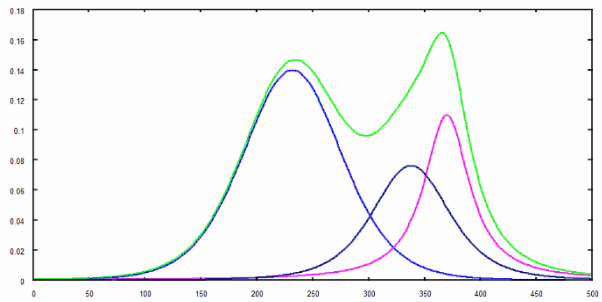

Fig. 8: As in the Figure 5, the green curve here given is the curve that we will use for the new fitting simulations. The three q-Gaussians are corresponding to D1 (q=1.2), D3 (q=1.4) and G (1.8). Note the different right wing.

Here in the following Figures the results of the best fit (constrained and unconstrained).

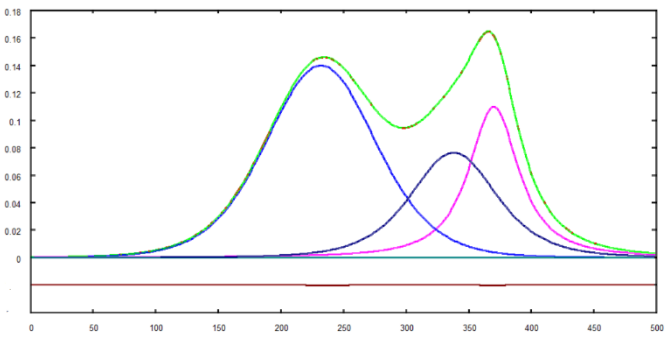

Fig. 9: Red curve is the curve to fit, and the green curve is the best fit (constrained q parameters). Curves are indistinguishable. The components are given by blue and pink lines. Fitting parameters are: q=1.2, C=0.13966, σ=42.416 (D1), q=1.8, C=0.10966, σ=17.416 (G) and q=1.4, C=0.0763, σ= 32.083 (D3). The sum of the squares of the deviations is $\Delta^2 = 3.1 \times 10^{-6}$.

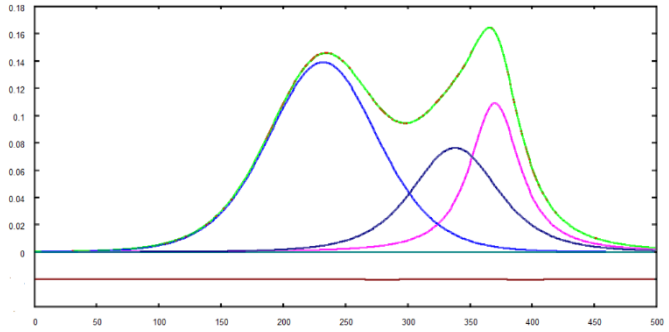

Fig. 10: Red curve is the curve to fit and the green curve is the best fit (unconstrained q). Fitting parameters are: q=1.20, C=0.13900, σ=42.583 (D1), q=1.7625, C=0.1096, σ=17.583 (G) and q=1.4375, C=0.07633, σ= 32.083 (D3). The sum of the squares of the deviations is $\Delta^2 = 8.2 \times 10^{-6}$.

Comparing the results in the Figures 9 and 10, we could conclude that an uncertainty of ±0.05 is given about the value of parameter q obtained from fitting procedure.

7. Two components

Let us consider a simulation, where the D3 peak has a null contribution. How is reacting the unconstrained simulation? It reacts in a very positive manner.

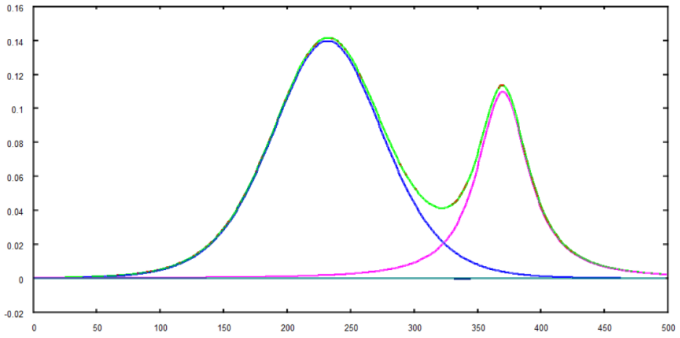

Fig. 11: Red curve is the curve to fit, obtained just with D1 and G components. The green curve is the best fit (unconstrained q). Fitting parameters are: q=1.200, C=0.13966, σ=42.4166 (D1), q=1.800, C=0.10966, σ=17.5833 (G) and q=1.862, C=-3.333 x 10^{-4} *, σ= 7.250 (D3). The sum of the squares of the deviations is* $\Delta^2 = 4.0 \times 10^{-6}$ *. The results regarding D3 tell us that it does not exist for sure.*

8. Moving D3

In the previous simulations we have maintained fixed the positions of the centers of the bands. Now, let us relax this condition, and assume that the position of D3 can change. To understand the role of the position of the center of this peak, we use the fit with unconstrained q parameters.

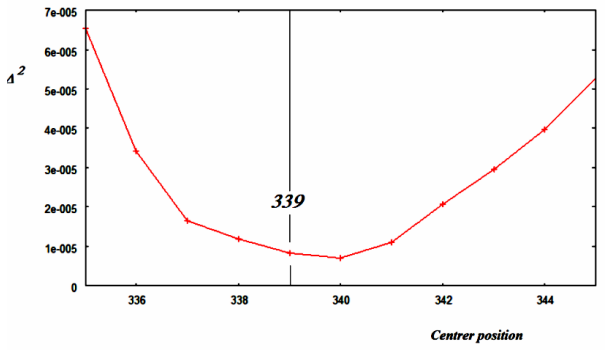

Fig.12: The position of the center of the peak D3 in the fitting is changed. The best fit is given at position 340 (399 in the Figures 5 and 8). However, the minimum is quite flat and therefore the position of the center can be assume given with an uncertainty of ±2.

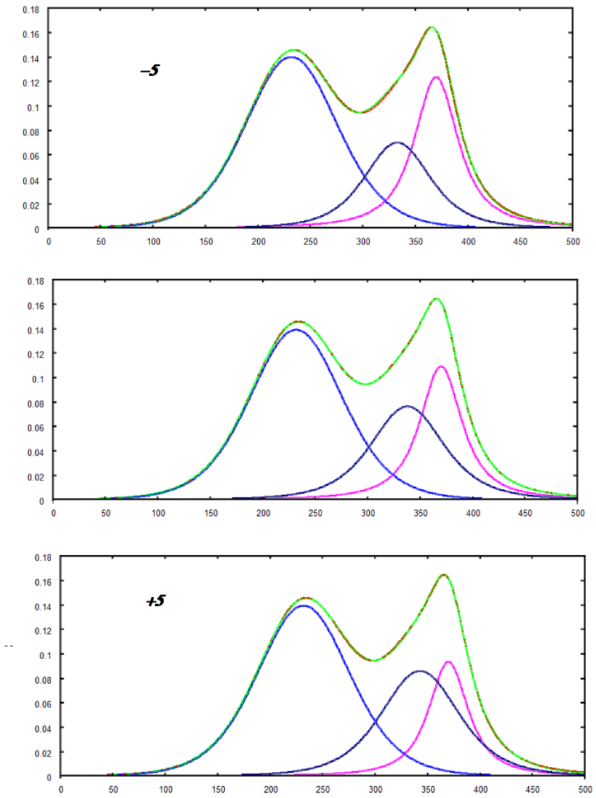

To observe the effect of position of D3 center line, let us move it to the right and to the left of 5 units, maintaining fixed the positions of D1 and G. The effect of the shift of D3 in the fitting results regarding the two components G and D3 is shown in the three plots of Figure 13.

Fig. 13: Changing the position of D3 band of -5 (top) and +5 (bottom) with respect to the reference position (middle), the values of the sum of the squares of deviations change according to the previous Figure 12. Note that the G band quite changes accordingly.

9. Gaussian and Lorentzian functions

What happens if we use Gaussian and Lorentzian functions instead of the q-Gaussians? Results are given in the following figures. We use for the fit Gaussian-like functions, that is q-Gaussians with q=1.01, and Lorentzian functions (q=2).

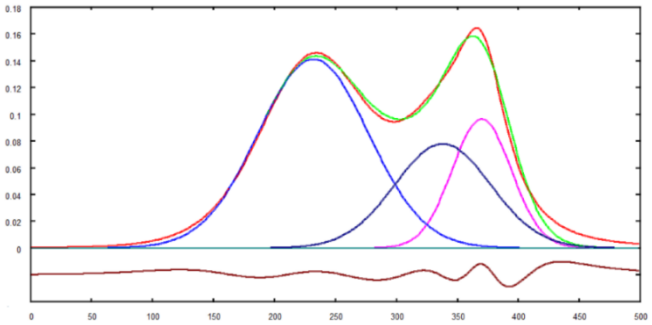

Fig. 14: Here we use three q-Gaussians, with the same q value equal to 1.01, for the fit of the red curve. The positions of the centers of these Gaussians have been fixed as that of the Figure 8. The green curve is the best fit. In the lower part of the image, the difference between the red curve and the green curve is given. There is a great difference due to the wings of the Gaussians. $\Delta^2 = 7.83 \times 10^{-3}$ *. Fitting parameters are: C=0.14100, σ=45.250 (D1), C=0.096, σ=24.25 (G) and C=0.0776, σ= 39.41 (D3).*

Let us relax the condition of the fixed position of the center of D3. We move it to the right, in the position 399+15. The result is given in the following Figure 15, and it is displaying a better approximation, but the relative weights of D3 and G are quite different.

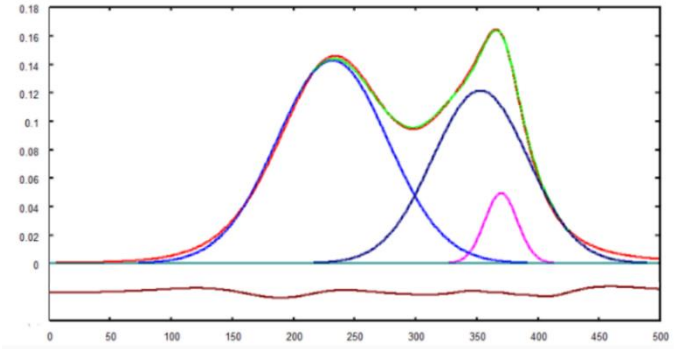

Fig. 15: Three q-Gaussians with the same q value equal to 1.01. The positions of the centers of D1 and G are fixed. The center of D3 is at 399+15. The green curve is the best fit. In the lower part of the image, the difference between the red curve and the green curve is given. $\Delta^2 = 2.43 \times 10^{-3}$ *. Fitting parameters are: C=0.14266, σ=45.333 (D1), C=0.049, σ=13.33 (G) and C=0.1213, σ= 39.16 (D3).*

In the approximations given by the iterative approach, changing the positions of D1 and G does not produce a better result. However, let us stress the difference of relevance of D3 with respect to G shown in the Fig.15. In the following Figures, we continue with fitting simulations, introducing Lorentzian functions. Let us consider two Gaussians for D1 and G, and a Lorentzian function for D3. The positions of the centers of the peaks are the same as in the Figure 8.

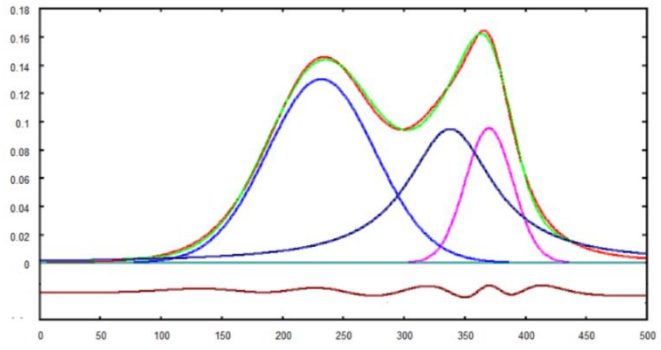

Fig. 16: Here we use for fitting two q-Gaussians with the same q value equal to 1.01 for D1 and G, and a Lorentzian function for D3. The positions of the centers of these Gaussians have been fixed as that of the Figure 8. The green curve is the best fit. In the lower part of the image, the difference between the red curve and the green curve is given. $\Delta^2 = 2.08 \times 10^{-3}$ *. Fitting parameters are: C=0.1300, σ=44.33 (D1), C=0.095, σ=19.5 (G) and C=0.095, σ= 30.66 (D3).*

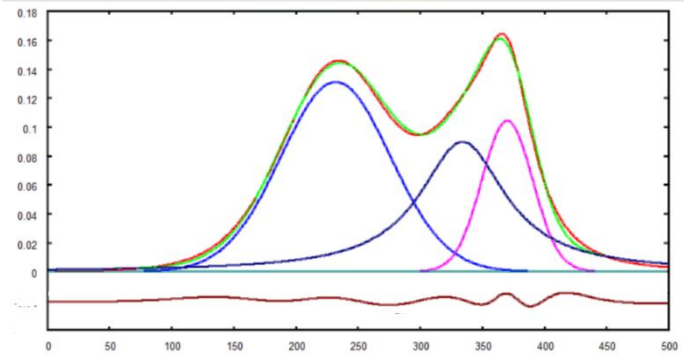

Fig. 17: Let us consider, as in the previous figure, two q-Gaussians with the same q value equal to 1.01 for D1 and G, and a Lorentzian function for D3. The position of the center of G3 is shifted to the left of 4 units. The green curve is the best fit. In the lower part of the image, the difference between the red curve and the green curve is given. $\Delta^2 = 1.98 \times 10^{-3}$ *. Fitting parameters are: C=0.1310, σ=44.083 (D1), C=0.104, σ=20.41 (G) and C=0.089, σ= 29.75 (D3).*

Comparing the two last figures, Fig. 16 and 17, we can see that a rather small shift of the center of D3 is producing an evident change in the G peak. The change of Δ^2 is negligible. We can also compare the behavior of the D3 Lorentzian band (Fig. 16 and 17) to that of the D3 q band in Fig.13: they are similar but in opposite trends.

For the fitting simulations, we limited the sampling to the range displayed by the x-axis of the figures. In the case of the use of Gaussian and Lorentzian functions, an expanded range is relevant for sure. However, if the curve to be fitted is composed by components which have a behavior intermediate between Gaussian and Lorentzian, it is better to use q-Gaussian functions.

10. Fitting data

Simulations tell that we can distinguish the results obtained by means of the q-Gaussians line shapes from those deduced using Gaussian and Lorentzian functions. We can also determine the value of q parameter for each component, and the position of its center. Of course, if the synthetic "experimental" curve that we use for the simulation is produced by pure Gaussian and Lorentzian functions, the fitting by means of q-Gaussians is suitable too, being Gaussian and Lorentzian functions two cases of q-Gaussians. Then, to obtain further information about the role of q-Gaussians in Raman fitting, we must pass to the analysis of true experimental data. This is the subject of the second part of the proposed research work.

11. Synthetic Organic Pigments

Let us start from a spectrum of SOPRANO database (https://soprano.kikirpa.be/index.php?lib=sop , Fremout & Saverwyns, 2012). The first Raman spectrum of this database that we consider is named PO72. It is a synthetic pigment benzimidazolone (Creative Common Attribution – NonCommercial - NoDerivatives 4.0 License), https://soprano.kikirpa.be/index.php?lib=sop&id=PO72_A_785_kikirpa , analyst Wim Fremout. The first peak considered is that at 1595 cm^{-1}. Here in the following Figures 18 and 19, the data and the best fit. The agreement is remarkable. The largest component has q=1.65.

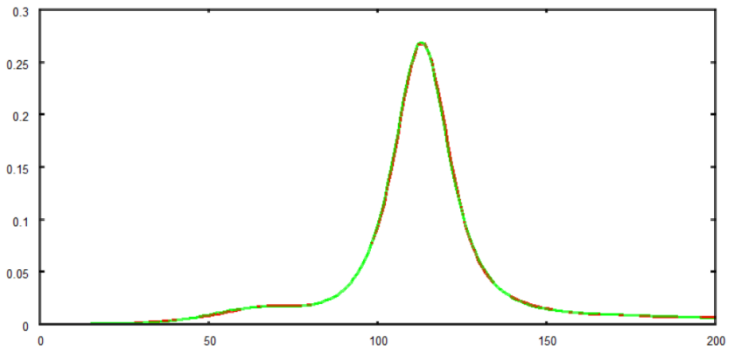

Fig. 18: Best fit (in green) of the spectral data (in red) regarding a peak of the SOPRANO PO72 spectrum. Arbitrary units on both axes.

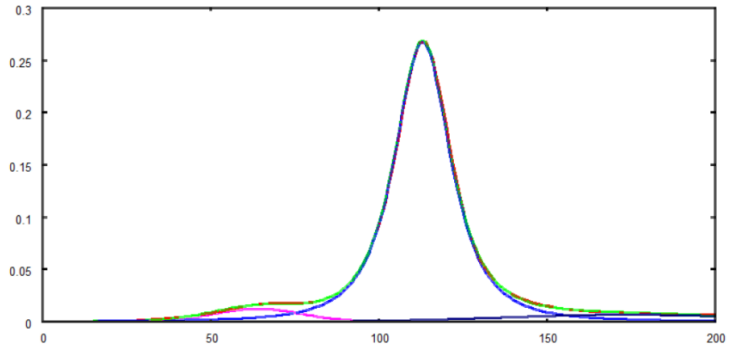

Fig. 19: Data, best fit and components. . $\Delta^2 = 2.43 \times 10^{-4}$ .of the same peak given in Fig.18. The components are three. From left to right, the fitting parameters are: q=1.01, C=0.01223, σ=13.15; q=1.65, C=0.2673, σ=7.45 (large peak); and q=1.01, C=0.0067, σ= 36.25.

What happens if we use the Lorentzian function for the main peak? Here the result in the Fig.20.

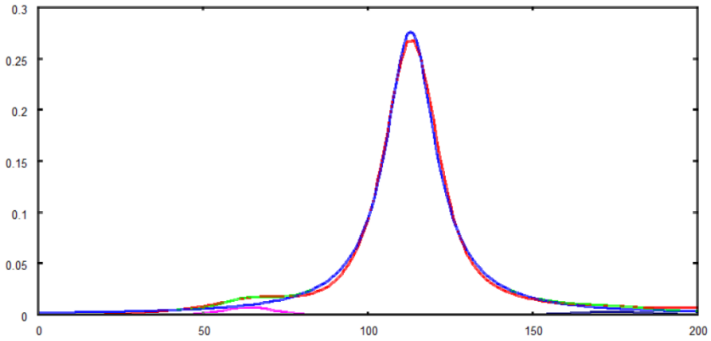

Fig. 20: Data, best fit and components. $\Delta^2 = 1.93 \times 10^{-3}$. The components are from left to right Gaussian, Lorentzian and Gaussian. Note the difference in both kernel and wings. The fitting with the q-Gaussian function, given in Fig.19, is perfect, not that obtained with a Lorentzian function.

Another spectrum that we consider is PBk31 (aniline black), available https://soprano.kikirpa.be/index.php?lib=sop&id=PBk31_A_785_kikirpa . The Raman shift between the two peaks is of 1579 cm^{-1}.

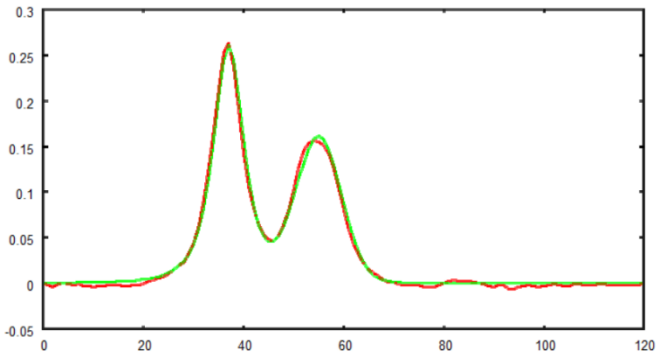

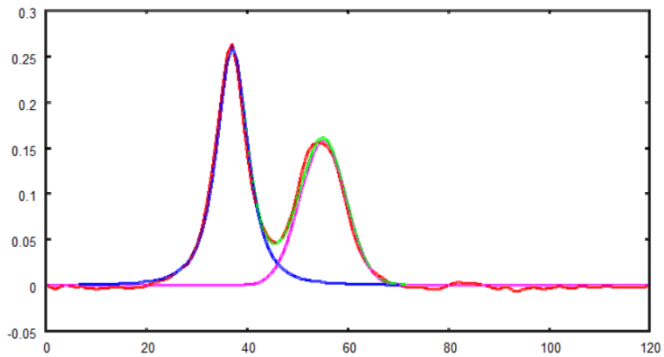

Fig. 21: Data, best fit and components. $\Delta^2 = 2.33 \times 10^{-3}$. The components are two. From left to right, the fitting parameters are: q=1.60, C=0.260, σ=2.76 and q=1.01, C=0.158, σ=4.50.

Then, let us consider PBr42, Cromophtal Brown RBN, available at the link https://soprano.kikirpa.be/index.php?lib=sop&id=PBr42_A_785_kikirpa . The peaks of the Raman shift are at 955 and 983 cm^{-1} respectively.

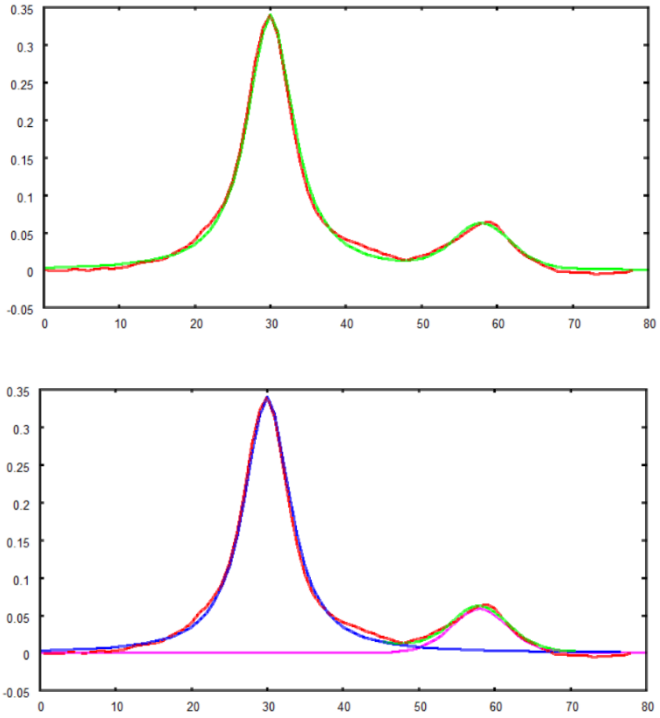

Fig. 22: Data, best fit and components. $\Delta^2 = 2.25 \times 10^{-3}$. The components are two. From left to right, the fitting parameters are: q=1.875, C=0.341, σ=2.633 and q=1.125, C=0.059, σ=3.63.

12. Baseline or component?

Of the spectrum PV27, https://soprano.kikirpa.be/index.php?lib=sop&id=PV27_A_785_kikirpa, which is the violet Triarylcarbonium, we consider the two peaks at 1600 cm^{-1}. Here we can investigate a further problem, related to the role of the baseline. Let us start with the best fit with two components given in the following figure. As for the previously proposed fits, we used the baseline corrected data given by the web page.

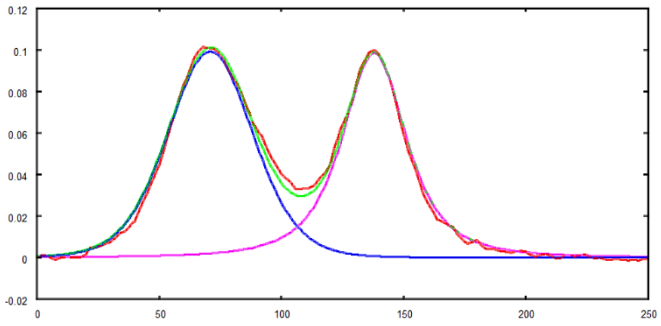

Fig. 23: Data, best fit and components. . $\Delta^2 = 1.28 \times 10^{-3}$. The components are two. From left to right, the fitting parameters are: q=1.162, C=0.0992, σ=16.916 and q=1.612, C=0.0984, σ=11.75..

The agreement is good. However, we have a small difference in the part of the spectrum between the two peaks and about the vertex of the first peak. To understand why there are these differences, let us consider the original data too. They are given in the following figure. We can use the original data and choose a local linear baseline (the green line), to have a different baseline correction.

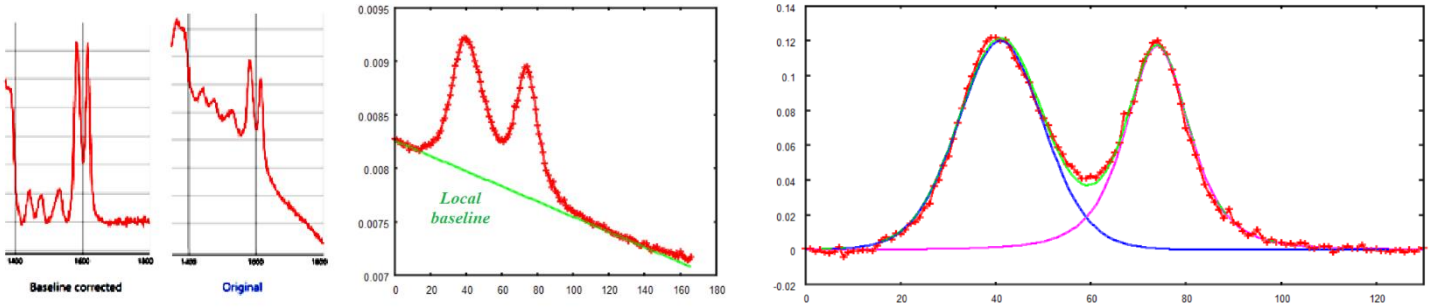

Fig. 24 – On the left, the corrected and the original data as given by the web page of Soprano. In the middle, the original data and a local linear baseline here used for fitting, to obtain a different best fit. On the right, the best fit with two components, with the data corrected with the local baseline. We have a better agreement. Parameters q are slightly changed into 1.12 and 1.48 respectively.

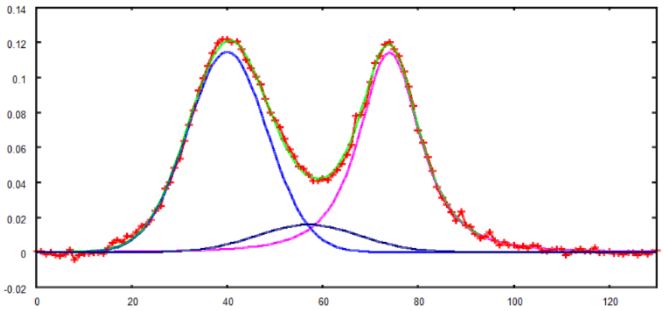

Fig. 25: Best fit with three components. The q parameters of the two large peaks are 1.02 and 1,6 respectively.

In the Fig.24, we have proposed the best fit with two components. We can further investigate, for the same data, the role of a third component included in the fit. The result is given in the Fig.25. For the data here considered, and about the fitting with two or three components, a question can be posed: is the third component strictly necessary, or is it simply the result of an approximation in the choice of the baseline? We have used a local linear baseline, but a non-linear baseline could give us a better result, eliminating the necessity of the third component.

13. Other peaks

Of the spectrum PV27, https://soprano.kikirpa.be/index.php?lib=sop&id=PV27_A_785_kikirpa, let us consider the fitting of other peaks (baseline corrected).

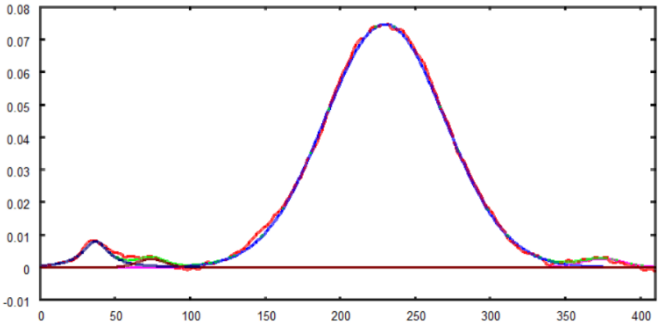

Fig. 26: Best fit with three components. The q parameter of the large peak (216 cm^{-1}) is 1.012 (a Gaussian).

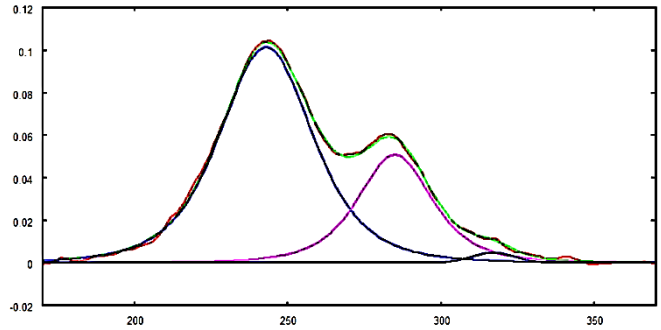

Fig. 27: Best fit with three components. The largest peak is at the Raman shift of 420 cm^{-1}. The q-parameters of the blue and pink lines are 1.40 and 1.46 respectively.

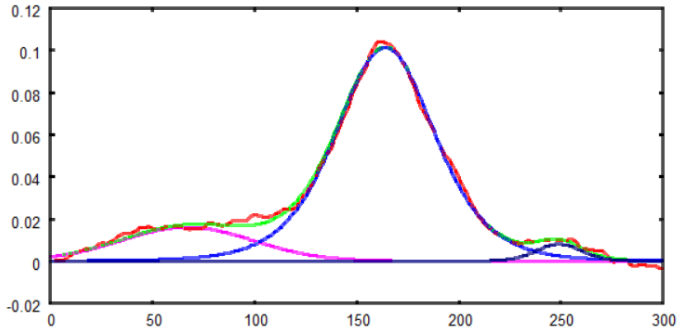

Fig. 28: Best fit with three components. The largest peak is at the Raman shift of 1180 cm^{-1}. The q-parameter of the largest blue peak is 1.30.

References

1. Application Note. Characterizing graphene with Raman spectroscopy. Available https://web.archive.org/web/20220815105344/https://assets.thermofisher.com/TFS-Assets/MSD/Application-Notes/AN53174-characterizing-graphene-raman-spectroscopy.pdf
2. Bartoli, M., & Giorcelli, M. (Eds.). (2022). Recent Perspectives in Pyrolysis Research. IntechOpen Editions.
3. Brassard, P., Godbout, S., Lévesque, V., Palacios, J. H., Raghavan, V., Ahmed, A., Hogue, R., Jeanne, T., & Verma, M. (2019). Biochar for soil amendment. In Char and carbon materials derived from biomass (pp. 109-146), Elsevier, 2019
4. Das, C., Tamrakar, S., Kiziltas, A., & Xie, X. (2021). Incorporation of biochar to improve mechanical, thermal and electrical properties of polymer composites. Polymers, 13(16), 2663

5. De Abreu, W. V., Maciel, J. M., Martinez, A. S., Gonçalves, A. D. C., & Schmidt, L. (2022). Doppler Broadening of Neutron Cross-Sections Using Kaniadakis Entropy. Entropy, 24(10), 1437.
6. Demtröder, W. (1985). Laser spectroscopy: Basic concepts and instrumentation. Springer Verlag.
7. Fremout, W., & Saverwyns, S. (2012). Identification of synthetic organic pigments: the role of a comprehensive digital Raman spectral library. Journal of Raman spectroscopy, 43(11), 1536-1544.
8. Giorcelli, M., Das, O., Sas, G., Försth, M., & Bartoli, M. (2021). A review of bio-oil production through microwave assisted pyrolysis. Processes, 9(3), 561.
9. Guedes, G., Palma, D. A., & Gonçalves, A. C. (2019). A deformed Doppler Broadening Function considering the Tsallis speed distribution. Annals of Nuclear Energy, 128, 414-421.
10. Han, J., & Kim, H. (2008). The reduction and control technology of tar during biomass gasification / pyrolysis: an overview. Renewable and sustainable energy reviews, 12(2), 397-416
11. Howarth, D. F., Weil, J. A., & Zimpel, Z. (2003). Generalization of the lineshape useful in magnetic resonance spectroscopy. Journal of Magnetic Resonance, 161(2), 215-221.
12. Jain, V., Biesinger, M. C., & Linford, M. R. (2018). The Gaussian-Lorentzian Sum, Product, and Convolution (Voigt) functions in the context of peak fitting X-ray photoelectron spectroscopy (XPS) narrow scans. Applied Surface Science, 447, 548-553.
13. Koksharov, Y. A. (2015). Application of Tsallis functions for analysis of line shapes in electron magnetic resonance spectra of magnetic nanoparticles. Physics of the Solid State, 57, 2011-2015.
14. Li, Y. (2009). Using the Tsallis distribution and the fractional differentiation to resolve the overlapping bands. Analytical and bioanalytical chemistry, 394, 637-645.
15. Li, Y., Zhang, Y., & Tang, H. (2010). Tsallis model-based separation of overlapped peak signals. Science China Information Sciences, 53, 823-832.
16. Meier, R. J. (2005). On art and science in curve-fitting vibrational spectra. Vibrational spectroscopy, 2(39), 266-269.
17. Naudts, J. (2009). The q-exponential family in statistical physics. Central European Journal of Physics, 7, 405-413.
18. Nienhuis, G., & Schuller, F. (1977). Collision and Doppler broadening of fluorescence and Raman scattering from atoms. Physica B+ C, 92(3), 409-420.
19. Ok, Y. S., Uchimiya, S. M., Chang, S. X., & Bolan, N. (Eds.). (2015). Biochar: Production, characterization, and applications. CRC press.
20. Ok, Y. S., Tsang, D. C., Bolan, N., & Novak, J. M. (Eds.). (2018). Biochar from biomass and waste: fundamentals and applications. Elsevier
21. Raman, C. V. (1931). Doppler effect in light-scattering. Nature, 128(3232), 636-636.
22. Rényi, A. (1955). On a new axiomatic theory of probability. Acta Mathematica Hungarica, 6(3-4), 285-335.
23. Sadezky, A., Muckenhuber, H., Grothe, H., Niessner, R., & Pöschl, U. (2005). Raman microspectroscopy of soot and related carbonaceous materials: Spectral analysis and structural information. Carbon, 43(8), 1731-1742.
24. Sharifi, M., & Parvazian, A. (2015). Stimulated Raman scattering in nonextensive statistics. Physica A: Statistical Mechanics and its Applications, 440, 176-184.
25. Sousa, D. V. D., Guimarães, L. M., Felix, J. F., Ker, J. C., Schaefer, C. E. R., & Rodet, M. J. (2020). Dynamic of the structural alteration of biochar in ancient Anthrosol over a long timescale by Raman spectroscopy. PloS one, 15(3), e0229447.
26. Sparavigna, A. C. (2022). Entropies and Logarithms. Zenodo. DOI 10.5281/zenodo.7007520
27. Sparavigna, A. C. (2023a). q-Gaussian Tsallis Line Shapes and Raman Spectral Bands. International Journal of Sciences, 12(03), 27-40.
28. Sparavigna, A. C. (2023b). q-Gaussian Tsallis Functions and Egelstaff-Schofield Spectral Line Shapes. International Journal of Sciences, 12(03), 47-50.
29. Tagliaferro, A., Rovere, M., Padovano, E., Bartoli, M., & Giorcelli, M. (2020). Introducing the novel mixed gaussian-lorentzian lineshape in the analysis of the raman signal of biochar. Nanomaterials, 10(9), 1748.
30. Townsend, R. (2008). Astronomy 310, Stellar Astrophysics, Fall Semester 2008, Lecture Notes, https://web.archive.org/web/20230421054452/http://user.astro.wisc.edu/~townsend/resource/teaching/astro-310-F08/17-line-profiles-2.pdf
31. Tsallis, C. (1988). Possible generalization of Boltzmann-Gibbs statistics. Journal of statistical physics, 52, 479-487.

32. Tsallis, C. (1995). Some comments on Boltzmann-Gibbs statistical mechanics. Chaos, Solitons & Fractals, 6, 539-559.
33. Tsallis, C., Levy, S. V., Souza, A. M., & Maynard, R. (1995). Statistical-mechanical foundation of the ubiquity of Lévy distributions in nature. Physical Review Letters, 75(20), 3589.
34. Umarov, S.,Tsallis, C., Steinberg, S. (2008). On a q-Central Limit Theorem Consistent with Nonextensive Statistical Mechanics. Milan J. Math. Birkhauser Verlag. 76: 307–328. doi:10.1007/s00032-008-0087-y. S2CID 55967725.
35. Yasim-Anuar, T. A. T., Yee-Foong, L. N., Lawal, A. A., Farid, M. A. A., Yusuf, M. Z. M., Hassan, M. A., & Ariffin, H. (2022). Emerging application of biochar as a renewable and superior filler in polymer composites. RSC advances, 12(22), 13938-13949.